Raman Spectrum of KTa$_{0.64}$Nb$_{0.36}$O$_3$[†]

S. K. Manlief[*] and H. Y. Fan

Department of Physics, Purdue University, Lafayette, Indiana 47907

(Received 3 January 1972)

Raman scattering from the mixed crystal KTa$_{0.64}$Nb$_{0.36}$O$_3$ ($T_c \approx 10$ °C) has been investigated as a function of temperature in the paraelectric and single-domain-ferroelectric phases. The phonon spectrum was found to correspond predominantly to that of the host lattice of KTaO$_3$. Significant effects due to the mixed nature of the crystal were found. In the ferroelectric phase, first-order lines were observed with symmetry properties forbidden for an ideal perovskite structure. Also, two Raman lines in the ferroelectric phase are attributed to local modes associated with the Nb ions in the lattice. In the paraelectric phase, lines observed at 202 and 279 cm^{-1} persisted as first-order structures. The behavior of the 279-cm^{-1} line was found to be consistent with a reduction of the phonon symmetry from F_{2u} to F_2, which could be caused by a relaxation of the inversion symmetry of the cubic lattice. The persistence of the 202-cm^{-1} line cannot be accounted for by the loss of inversion symmetry and may be due to the relaxation of translational symmetry. The shape of the 202-cm^{-1} peak shows a Fano-type interference. First-order structures occurred also at 175 and 436 cm^{-1}, and are attributed to zone-boundary phonons. First-order scattering was induced in the paraelectric phase by the application of an electric field to the sample. For comparable values of polarization, the intensity of the induced first-order scattering measured just above the transition temperature was found to be substantially less than the intensity of the spontaneous first-order scattering measured just below the transition temperature. Existing theory predicts that the spontaneous and induced scattering intensities should be nearly equal for these conditions.

I. INTRODUCTION

In the perovskites, the lowest-frequency transverse-optical phonon or soft ferroelectric mode is closely associated with the lattice instability at the phase transitions.[1,2] Consequently, the lattice dynamics of this class of materials has been of great interest. Recently, several Raman-scattering studies of the lattice dynamics of mixed perovskite systems have been reported. These investigations have all been on either powdered or ceramic samples or multidomain single crystals for which well-defined scattering geometries are not possible. This situation prevents a detailed study of the symmetries of the contributing phonons and limits the amount of information that can be obtained. An important assumption made in the analysis of the Raman measurements on powdered and ceramic materials is that the selection rules for the pure perovskite structure are obeyed for the mixed systems.[3,4] The general validity of this assumption is questionable; e. g., significant effects due to the relaxation of selection rules have been observed in heavily doped[5,6] and mixed alkali halide[7] crystals. In this paper we report measurements of the Raman spectrum of the mixed perovskite crystal KTa$_{0.64}$Nb$_{0.36}$O$_3$ (KTN) in the paraelectric and single-domain-ferroelectric phases using well-defined scattering geometries so that the phonon symmetries can be determined for the mixed perovskite system.

The multidomain single-crystal studies of KTN have been confined primarily to investigations of the soft mode. In KTN, Todd[8] has studied the behavior of the soft mode as a function of composition. He found that the soft mode is heavily overdamped in the tetragonal and orthorhombic phases for all compositions. In the rhombohedral phase, the damping depends upon the thermodynamic order of the phase transition. No results for phonons other than the soft mode were reported. Perry and Tornberg[9] and Davis[10] have reported preliminary results of Raman studies on KTN. However, no data or spectra are given and their comments are limited to general statements.

We also report measurements of first-order scattering induced in the cubic phase by the application of an electric field along a crystal axis of the sample. Using both pulsed and ac field modulation, Fleury and Worlock[11,12] have induced first-order Raman scattering in cubic KTaO$_3$ and SrTiO$_3$, although not all the phonons could be observed. Theoretical investigations of the induced first-order scattering efficiency have been made by Dvořák[13] and, more recently, by Wemple and DiDomenico.[14] These results indicate that, for comparable polarization, the intensity of the induced first-order scattering measured just above the ferroelectric transition temperature should be nearly equal to the intrinsic or spontaneous first-order intensity measured just below the transition temperature. There have been no measurements of the induced scattering in the cubic phase of a material which has a phase transition to compare the induced first-order intensity with the spontaneous first-or-

der intensity measured in the ferroelectric phase.

II. EXPERIMENTAL APPARATUS AND SAMPLE PREPARATION

The 4880-Å line of an argon-ion laser was used as the excitation source. The polarization vector of the laser light was rotated with a quartz half-wave plate. The laser beam was focused into the sample with a 150-mm-focal-length lens and the scattered light collected at 90°. To increase the collection efficiency, the image of the scattering filament in the sample was rotated parallel to the monochromator slits with a dove prism. The polarization of the scattered light was analyzed with a sheet polarizer placed in front of the dove prism. Two synchronously driven, single-pass Perkin-Elmer grating monochromators were used as the monochromator system. For similar spectral slits, the stray light rejection of this double system was comparable to that of commercial double monochromators. An EMI 9558 photomultiplier (S-20 photocathode) cooled to approximately $-50\,°C$ was used as the detector. For the measurements of the intrinsic scattering and the dc-field-induced scattering, phase-sensitive detection was used with the incident laser radiation chopped at 480 Hz. The technique of Fleury and Worlock[11] was used for the ac-modulated-field-induced scattering.

The KTN samples used were obtained from Union Carbide Corp. and had a tantalum concentration of approximately 64%. The temperatures at the cubic-tetragonal and the tetragonal-orthorhombic phase transitions were 10.5 and $-36\,°C$, respectively. The crystals were highly insulating, with a resistivity in excess of 5×10^{12} Ω cm. The samples were cut into rectangular parallelepipeds with (100) faces and the optical surfaces ground and polished. Electrical contacts were made by evaporating gold on opposite surfaces which were ground flat and parallel. For the measurements in the ferroelectric phase, the crystals were poled into a single-domain state by slowly cooling the sample in vacuum from approximately 25 °C above the transition temperature with an electric field of approximately 7.5 kV/cm applied along a (001) axis. This procedure yielded good-quality single-domain samples as determined from optical measurements and by measurements of the dielectric constant.

The sample temperature was varied with a heating element mounted on the tailpiece of a Dewar cooled with a dry-ice–alcohol mixture. The temperature of the sample during the measurement was determined by measuring the sample capacitance and using a capacitance-versus-temperature-calibration curve obtained with no light on the crystal.

III. SELECTION RULES FOR PEROVSKITE STRUCTURE

A. Ideal Perovskite Structure

In the first-order Raman effect, wave-vector conservation requires that the magnitude of the wave vector of phonons participating in the scattering process be very small compared to the dimensions of the Brillouin zone. Thus, as a first approximation, only the zone-center phonons need be considered for determining the selection rules for Raman activity. Proper account should be taken of the polarization (or ionic displacements) of those phonons that are simultaneously infrared active.[15,16] The perovskite structure has five atoms and thus 15 degrees of freedom per unit cell. In the paraelectric phase, the crystal has cubic O_h symmetry; the zone-center phonons transform according to the irreducible representations $4F_{1u} + 1F_{2u}$, where F_{1u} and F_{2u} are each threefold degenerate. One of the F_{1u} normal modes corresponds to the acoustical branches and the other modes belong to the optical branches. The phonons are all of odd parity, so that they are first-order Raman inactive in the centrosymmetric phase, and one can observe only second-order spectra. Although Raman inactive, the F_{1u} modes are infrared active. The F_{2u} modes are both Raman and infrared inactive and are consequently called the silent modes.

In the tetragonal ferroelectric phase, the crystal symmetry is lowered to C_{4v} and all the phonons become Raman active in the first order. Each of the F_{1u} modes splits into modes of symmetry $A_1 + E$, where E is twofold degenerate, and the F_{2u} modes split into modes of $B_1 + E$ symmetry. The A_1 and E modes are infrared active, while the B_1 mode is infrared inactive. The long-range Coulomb fields associated with the infrared-active modes further split the degeneracies, so that, in the approximation that the electrostatic forces dominate over the lattice forces, there will be a maximum of three LO, eight TO, and an infrared-inactive B_1 mode for a given scattering geometry.

Two basic scattering geometries were used in this study: $X(bc)Y$ and $Z(bc)X$, where b and c can take on various values of x, y, and z. The notation $X(bc)Y$, for example, indicates that the laser light is incident along the X direction and polarized along the b direction while the scattered light is observed along the Y direction and analyzed along the c direction. The selection rules for first-order scattering are determined by the nonvanishing components of the polarizability derivative tensor

$$\left(\frac{\partial\alpha_{ij}}{\partial r_k}\right)_{r_k=0},$$

where r_k are the ionic-displacement coordinates. In the C_{4v}-symmetry phase, these tensors, for r_k parallel to the principal axes of the crystal, are

TABLE I. Selection rules for first-order Raman scattering in the C_{4v}-symmetry phase.

Spectrum	Phonon species allowed
$X(zz)Y$	$A_{1\,\text{TO}}$
$X(zx)Y$	$E_{\text{LO}}+E_{\text{TO}}$
$X(yz)Y$	$E_{\text{LO}}+E_{\text{TO}}$
$X(yx)Y$	no first order allowed
$Z(yz)X$	E_{TO}
$Z(yy)X$	$B_1+Q_{\text{LO}}+Q_{\text{TO}}$ [a]
$Z(xz)X$	$Q_{\text{LO}}+Q_{\text{TO}}$ [b]
$Z(xy)X$	no first order allowed

[a]Only the tensor components of the pure-symmetry-A_1 phonon contribute to the quasimode spectra.

[b]Only the tensor components of the pure-symmetry-E phonon contribute to the quasimode spectra.

given by Loudon[15] as

$$A_1(z)=\begin{bmatrix} a & 0 & 0 \\ 0 & a & 0 \\ 0 & 0 & b \end{bmatrix}, \quad B_1=\begin{bmatrix} c & 0 & 0 \\ 0 & -c & 0 \\ 0 & 0 & 0 \end{bmatrix},$$

$$E(x)=\begin{bmatrix} 0 & 0 & d \\ 0 & 0 & 0 \\ d & 0 & 0 \end{bmatrix}, \quad E(y)=\begin{bmatrix} 0 & 0 & 0 \\ 0 & 0 & d \\ 0 & d & 0 \end{bmatrix}.$$

The x, y, or z (z is parallel to the tetragonal c axis) following the infrared-active representations A_1 and E denotes the direction of phonon polarization. The selection rules for the scattering geometries used are listed in Table I. It was assumed that the electrostatic forces are much larger than the lattice forces, an approximation that is apparently valid for the perovskites,[12,17,18] so that the optical infrared-active modes are purely longitudinal (LO) or transverse (TO), independent of the direction of phonon propagation. For such modes, the polarizability derivative tensors listed above for the A_1- and E-symmetry phonons were transformed using a procedure due to Poulet,[16] so that the ionic displacements were either parallel or perpendicular to the phonon wave vector. The notations Q_{TO} and Q_{LO} in Table I are used to indicate that these modes have mixed A_1 and E symmetries, although they have pure TO or LO character. This type of mode is called a quasimode.

B. Mixed-Crystal Effects on Selection Rules

The discussion thus far has been confined to the case of the ideal perovskite structure. Some mechanisms that *may* give rise to anomalies in the symmetry properties of the Raman spectra for mixed perovskite systems will now be discussed. The KTN crystals used in this study may be considered approximately as a host lattice of $KTaO_3$ with some of the Ta ions randomly replaced by Nb. There is a possibility of observing localized

modes[19,20] associated with the Nb ions. To our knowledge, observations of local modes in the mixed perovskites have not been reported previously.

The mixed nature of the lattice lifts, in the strict sense, the symmetries of the lattice, in particular, the translational symmetry and, in the cubic phase, the inversion symmetry. The loss of translational symmetry relaxes the wave-vector selection rule so that the first-order phonons need not be restricted to the zone center[20,21] and contributions from phonons at symmetry points elsewhere in the Brillouin zone may be observed, depending upon the single-phonon density of states. The relaxation of the wave-vector selection rule also has the effect of introducing a general broadening of the phonon spectra.

The loss of inversion symmetry in the cubic phase has the effect of lowering the crystal symmetry from O_h to O. The F_{1u} and F_{2u} modes now transform according to F_1 and F_2, respectively. The F_1 modes remain both Raman and infrared inactive, while the F_2 modes are Raman active although infrared inactive. The polarizability derivative tensors for the triply degenerate F_2 modes are

$$\begin{bmatrix} 0 & 0 & 0 \\ 0 & 0 & e \\ 0 & e & 0 \end{bmatrix}, \quad \begin{bmatrix} 0 & 0 & e \\ 0 & 0 & 0 \\ e & 0 & 0 \end{bmatrix}, \quad \begin{bmatrix} 0 & e & 0 \\ e & 0 & 0 \\ 0 & 0 & 0 \end{bmatrix}.$$

The F_2 modes may possibly contribute to the $X(zx)Y$, $X(yz)Y$, and $X(yx)Y$ spectra but not to the $X(zz)Y$ spectrum.

IV. INTRINSIC RAMAN SCATTERING: RESULTS AND DISCUSSION

A. E-Symmetry Spectra

The scattering spectrum from the E-symmetry modes will first be considered in detail. Figure 1 shows the Stokes components of the $X(zx)Y$ spectrum to which both E_{TO} and E_{LO} modes contribute. Corresponding components with approximately the proper intensity ratio were observed in the anti-Stokes part of the spectrum. The solid curve applies to the ferroelectric phase and is characterized by the presence of sharp, well-defined first-order lines superposed on a second-order continuum of second-order scattering. The second-order spectrum shows considerable structure comparable in intensity, in some cases, to the weaker first-order lines. This is typical of the perovskites.[22,23] Consequently, considerable care must be exercised in differentiating first- and second-order structures. The dashed curve was obtained for the paraelectric phase and should represent only second-order spectrum if the ideal crystal selection rules are obeyed. It is observed that
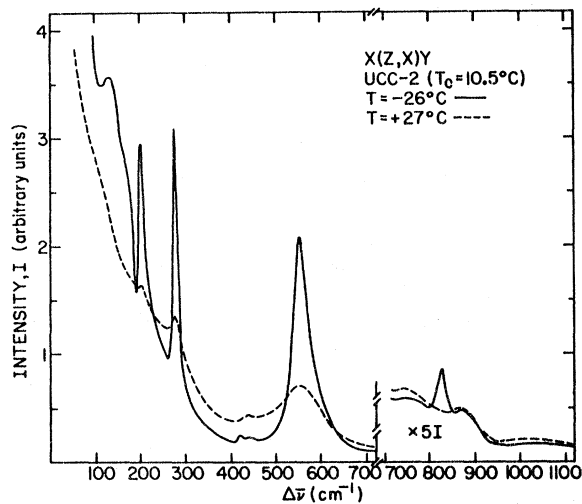
FIG. 1. Stokes components of the $X(zx)Y$ spectrum of KTN in the paraelectric and single–domain–ferroelectric phases. The dashed curve represents the spectrum in the paraelectric phase and the solid curve the spectrum in the ferroelectric phase.

some of the sharp first-order lines, although greatly reduced in intensity, do not disappear in the cubic phase, suggesting that some of the selection rules are relaxed in the mixed crystal. It is observed that, in most regions of the spectrum, the second-order continuum is relatively constant with temperature. The $X(yz)Y$ spectrum was, within experimental error, observed to be identical in shape and intensity with the $X(zx)Y$ spectrum. This is as expected, since the tensor components of the $E(x)$ and $E(y)$ modes are equal in magnitude.

The $X(zx)Y$ spectrum is replotted in Fig. 2 on a log scale to better illustrate the intensity variation with temperature. Although shown only to 1100 cm^{-1}, the spectrum was measured out to 1900 cm^{-1}. Beyond 1100 cm^{-1}, only a very broad, weak, second-order band centered at approximately 1720 cm^{-1} was observed. The wave-number shifts of the various peaks are shown in the figure with the structure assigned to second-order bands identified with parentheses. The general criterion that is used to determine the first-order lines is the disappearance of the peak intensity above the general background with little change in linewidth as the crystal is heated into the paraelectric phase. The TO and, in some cases, the LO character of the first-order lines can be determined by comparison with the $Z(yz)X$ spectrum as discussed below.

A Raman line at a particular frequency in the $X(zx)Y$ spectrum may contain scattering from either E_{TO} or E_{LO} phonons. It is also possible that the line may contain contributions from degenerate E_{TO} and E_{LO} modes, although this is not generally expected except for the silent modes.[17,18] Only

E_{TO} modes can be observed in $Z(yz)X$ scattering. The frequency of the near zone-center E_{TO} modes would not be expected to be significantly different for the directions of propagation parallel and perpendicular to the z axis. Thus, if the line observed in the $X(zx)Y$ spectrum is not present in the same frequency range in the $Z(yz)X$ spectrum, the scattering peak must be due to an E_{LO} mode. If the line is present in both spectra, there is a definite E_{TO} contribution; however, there may also be a degenerate E_{LO} contribution. Only LO modes can be observed in the $X+Z(yy)X-Z$ and the back-scattering $Z(yy)-Z$ spectra, so that these spectra could be used to resolve a possible E_{TO} and E_{LO} degeneracy. The notation $X+Z$ indicates light propagation in the xz plane at 45° to the x axis. These spectra were not measured for the following reasons. The $X+Z(yy)X-Z$ geometry requires that the wave vector of the exciting light inside the crystal be at an angle of 45° from the z axis. Since the transition temperature of the sample was below room temperature, it was necessary to apply a uniform electric field along the z axis to pole the crystal into a single-domain state prior to each measurement. This required the sample to be cut with surfaces perpendicular to the z axis and the surface to be covered with gold electrodes. In order to obtain good contacts, it was necessary to evaporate the gold onto ground surfaces. Although small semitransparent spots in the electrodes could be made to admit light into the crystal, it was not
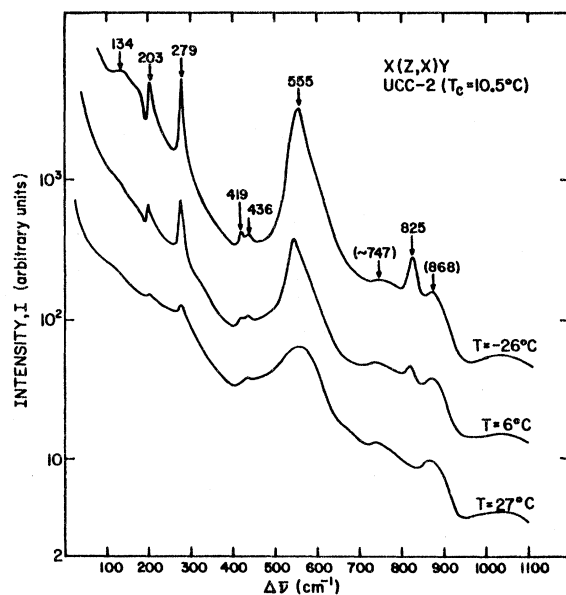

FIG. 2. $X(zx)Y$ spectrum measured at three different temperatures. The curves are not referred to the same baseline. Higher-order bands are identified with parentheses.
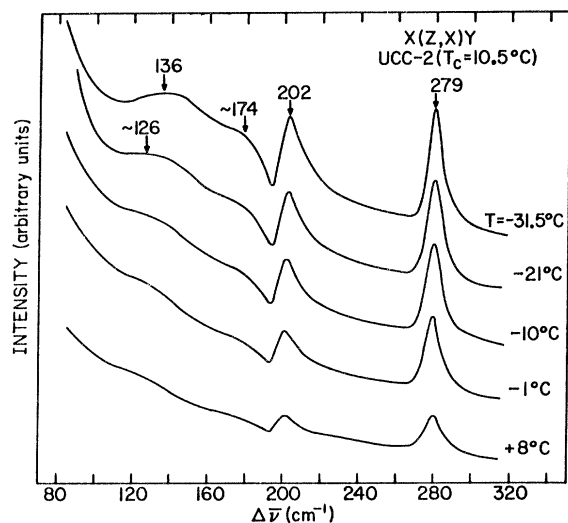
FIG. 3. Temperature dependence of the $X(zx)Y$ spectrum for $80 < \Delta\bar{\nu} < 320$ cm^{-1}. The curves are not referred to the same baseline.

possible to have the light propagating at a 45° angle with the z axis inside the sample because of refractive effects. The backscattering $Z(yy) - Z$ geometry was not attempted, since it was believed that reliable results would not be obtained owing to the refractive effect on the scattered light at the ground surface.

825-, 419-, *and* 134-cm^{-1} *lines*. These three lines vanish completely as the crystal is heated into the paraelectric phase and thus result from first-order scattering. The lines at 419 and 134 cm^{-1} are not present in the $Z(yz)X$ spectrum, so that the contributing phonons have LO character. The 825-cm^{-1} line is also present in the $Z(yz)X$ spectrum and thus has definite TO character, although, as discussed above, there may also be some LO contribution. It will later be argued that this line should correspond only to an LO mode and is apparently exhibiting anomalous behavior. The frequency of the LO phonon at ≈ 134 cm^{-1} decreases nearly linearly with increasing temperature, as shown in Fig. 3, at the rate of approximately 1 cm^{-1}/°C. This structure is attributed to a local mode associated with the Nb ions as discussed later.

202- *and* 279-cm^{-1} *lines*. These two lines seen in Fig. 3 do not vanish at the phase transition but persist in the cubic phase as shown in Fig. 2. The complete disappearance of the 134-, 419-, and 825-cm^{-1} first-order peaks in the cubic phase eliminates the possibility that the persistence of these two lines is of some spurious origin. The peak intensities above background and the half-widths of the two lines are plotted as functions of temperature in Figs. 4 and 5. The intensities of both lines de-

crease rapidly as the transition is approached. Above the transition in the cubic phase, the 202-cm^{-1} line continues to decrease slowly in intensity, finally vanishing at 60 °C. The 279-cm^{-1} line, in contrast, shows little further intensity variation persisting as a well-defined line. The half-widths of both peaks remain nearly constant over the full temperature range of ≈ 100 °C. What is observed, therefore, is not simply a thermal broadening effect on second-order structure but a large reduction of first-order intensity associated with the phase transition, with a small remainder due possibly to a relaxation of the selection rules in the cubic phase. Examination of the ferroelectric $Z(yy)X$ and the $X(zz)Y$ spectra shows that the 279-cm^{-1} line has B_1 but no A_1 symmetry, so that this line is derived from the cubic F_{2u} or silent mode. By elimination, this also implies that the 202-cm^{-1} line is associated with one of the cubic F_{1u} branches. In the cubic phase, the 279-cm^{-1} line is present in all the $X(bc)Y$ spectra except $X(zz)Y$. Its behavior is consistent with that of a zone-center, Raman-active F_2 mode which results from the F_{2u} mode owing to the relaxation of inversion symmetry as discussed in Sec. III. The relaxation of any one of the other point-group symmetries will not produce this behavior. The relaxation of inversion symmetry would not make the 202-cm^{-1} line first-order Raman active in the cubic phase. Obviously, some other mechanism is involved. One such possibility may be the loss of translational symmetry, which would allow contributions from other points in the Brillouin zone. The difference of the intensity variation of the two lines in the paraelectric phase may be due to the fact that the persistence results from the relaxation of different symmetries.

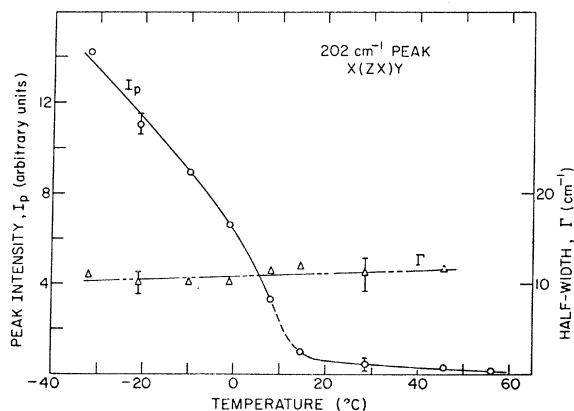*Line shape of* 202-cm^{-1} *peak*. Figure 3 shows

FIG. 4. Peak intensity and half-width as a function of temperature for the 202-cm^{-1} Raman line in the $X(zx)Y$ spectrum.
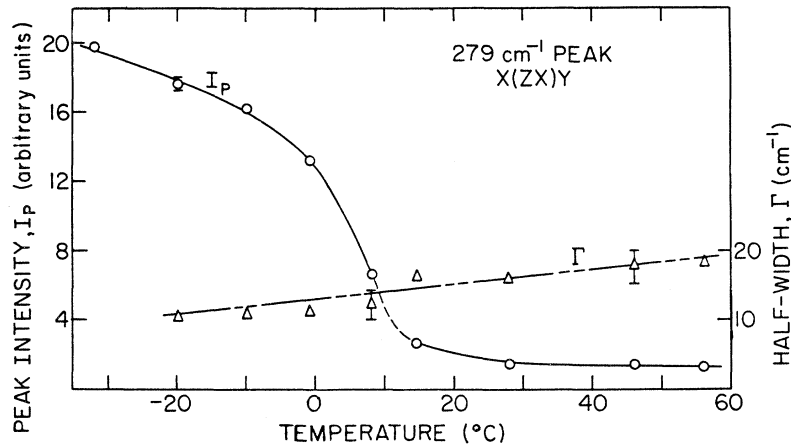
FIG. 5. Peak intensity and half-width as a function of temperature for the 279-cm^{-1} Raman line in the $X(zx)Y$ spectrum.

that the 202-cm^{-1} peak is markedly asymmetrical. A similar behavior has been observed for a TO phonon at 175 cm^{-1} in $BaTiO_3$, which was attributed by Rousseau and Porto[24] to an interference effect arising from a coupling of the single-phonon state to a two-acoustical-phonon state through anharmonic terms in the potential function. This interference mechanism was originally proposed by Fano.[25,26] Pinczuk, Burstein, and Ushioda[27] have suggested the possibility that the interference at 175 cm^{-1} in $BaTiO_3$ may also be due to the anharmonic coupling of the lowest-frequency zone-center TO mode with a higher-frequency zone-center TO mode via acoustical phonons. This mechanism was originally used by Barker and Hopfield[28] to interpret reflectivity spectra of $SrTiO_3$ and $BaTiO_3$. The 202-cm^{-1} line observed here is not the lowest-frequency TO mode. This fact and the very close similarity of the observed line shape and that of the Fano-type interaction suggest that this is the more probable type of interaction in this case.

555-cm^{-1} *line*. The line at ≈ 555 cm^{-1} has E_{TO} symmetry and its intensity variation with temperature is shown in more detail in Fig. 6. In the paraelectric phase, a broad two-phonon band peaked at approximately 560 cm^{-1} is observed. As the crystal is cooled into a single-domain-ferroelectric state, the intensity of this band increases in an asymmetrical fashion. A peak appeared at ≈ 545 cm^{-1} which increased in intensity with decreasing temperature and shifted slightly in frequency. The peak appears to correspond to a first-order E_{TO} peak, which is allowed for the $X(zx)Y$ spectrum. The asymmetry of the structure suggests that a weak interference effect of the Fano type is present here, although not to the extent that is shown by the 202-cm^{-1} line. In the $X(yx)Y$ spectrum, shown in Fig. 8, for which no first-order radiation is allowed in the ideal perovskite structure, the two-phonon band does not

change significantly when the crystal is cooled into the ferroelectric phase and no peak appeared.

Soft E_{TO} mode. The scattering close to the laser line is shown in Fig. 7 for the $X(yz)Y$ and $X(yx)Y$ spectra, each for two different temperatures, -30 and $+15\,°C$. These measurements were made with a spectral slit of ≈ 1 cm^{-1} to minimize the spuriously scattered Rayleigh light. In the ferroelectric phase at $T = -30\,°C$, the intensity of the $X(yz)Y$ spectrum for which first-order E-symmetry modes are allowed is greater than the intensity of the $X(yx)Y$ spectrum for which no first-order radiation is allowed. As the temperature was increased, the intensity of the $X(yz)Y$ spectrum decreased, while that of the $X(yx)Y$ spectrum remained constant. At the transition temperature and on into the paraelec-
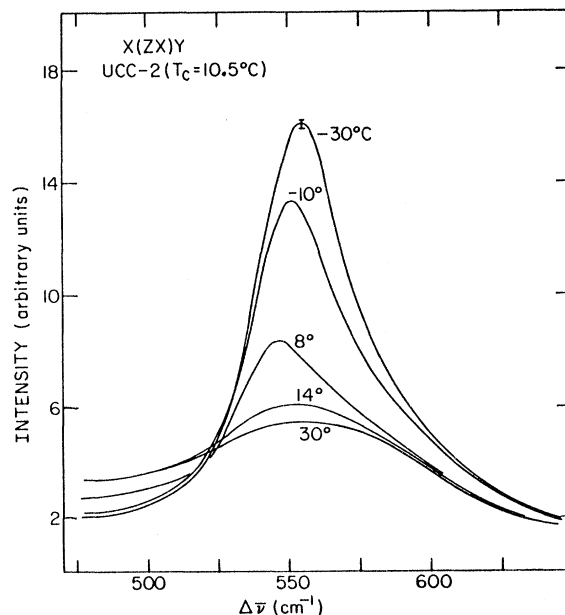

FIG. 6. Temperature dependence of the intensity of the 555-cm^{-1} E_{TO} Raman line.
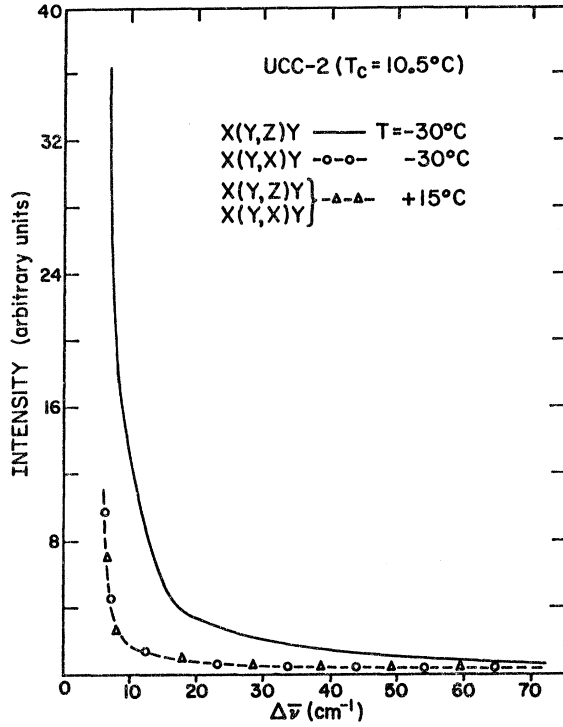
FIG. 7. Overdamped soft-E_{TO}-mode Raman spectrum in KTN. At $T = -30\,°C$ in the single-domain-ferroelectric phase, the solid curve is for the $X(yz)Y$ spectrum that allows E_{TO} scattering and the dashed curve is for the $X(yx)Y$ spectrum for which no first-order scattering is allowed. In the paraelectric phase, both spectra are represented by the dashed curve.

reported to be quite good, with an accuracy of $\pm 10\%$ claimed for the fitting parameters Γ and ω_{TO}.

The intensity per unit frequency interval of the soft mode in KTN at $T = -30\,°C$, which is taken to be the difference of the $X(yz)Y$ and the $X(yx)Y$ curves in Fig. 7, is not well represented by Eq. (1). At best, the undamped mode frequency and the damping constant could be estimated to be in the ranges 30–40 and 1.0–1.5 cm^{-1}, respectively. It will be shown, however, that the results of the quasimode measurements tend to confirm the range 30–40 cm^{-1} for the undamped mode frequency. The lack of a good fit may, in part, be due to dispersion effects introduced by the loss of translational symmetry in the mixed crystal. The dispersion of the soft-mode frequency in the perovskites is quite large. For example, at room temperature, the soft-mode frequency in $KTaO_3$ ranges from 85 cm^{-1} at the zone center to approximately 175 cm^{-1} at the zone boundary.[30] Thus, since wave vector is not strictly conserved in the mixed crystal, the phonons contributing to the soft-mode spectrum may not have a well-defined energy.

Forbidden symmetry lines in the $X(yx)Y$ spectrum. The $X(yx)Y$ spectrum for which no first-order contribution is allowed for the ideal perovskite structure is shown in Fig. 8. The intensity of this spectrum is generally constant with temperature in both the paraelectric and ferroelectric phases, indicating that it is predominantly second order. There is, however, a well-defined, for-

tric phase, both curves coincide and are given by the dashed curve. The difference of the two curves in the ferroelectric phase, then, represents first-order radiation of E_{TO} character as determined by comparison with the $Z(yz)X$ spectrum and is characteristic of a highly overdamped low-frequency mode. This is assigned to the soft E_{TO} mode. Todd[8] has previously reported this behavior for the soft E mode in multidomain KTN.

The soft E mode in $BaTiO_3$ is heavily damped[29] and has been reported by DiDomenico *et al.*[17] to appear in the Raman spectrum as a low-frequency wing extending out from the laser line as observed here for KTN. These authors fitted their spectra to a damped single-oscillator model in which the Raman-scattered light from the soft mode per unit frequency interval $dI_s/d\omega$ is given by the expression

$$\frac{dI_s}{d\omega} \propto \frac{\Gamma \omega_{TO}^3}{(\omega_{TO}^2 - \Delta\omega^2)^2 + 4\Gamma^2 \omega_{TO}^2 \, \Delta\omega^2} \; , \tag{1}$$

where Γ is the damping constant, ω_{TO} is the undamped mode frequency, and $\Delta\omega$ is the frequency deviation from the exciting laser line. The fit is
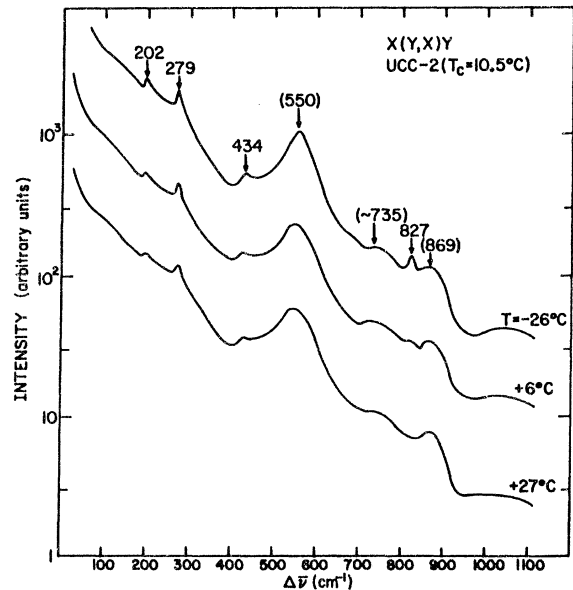

FIG. 8. $X(yx)Y$ spectrum measured at three different temperatures. The curves are not referred to the same baseline. Higher-order bands are identified with parentheses.

bidden, first-order peak at 827 cm^{-1} that vanishes at the phase transition. First-order forbidden lines in the ferroelectric phase are also observed at 202 and 279 cm^{-1}, which persist weakly in the paraelectric phase. There is no evidence of first-order scattering at 135, 419, and 555 cm^{-1} and the soft-mode region.

As in the $X(zx)Y$ spectra, the peak intensity above background of the 202-cm^{-1} line vanishes at approximately 60 °C, although the intensity decreases nearly linearly with increasing temperature, showing no change in slope at the transition as before. The existence of this line in the paraelectric phase was previously ascribed to the relaxation of translational symmetry. The 279-cm^{-1} line showed a similar linear variation of intensity in the ferroelectric phase; in the paraelectric phase, however, the intensity remained nearly constant with temperature. As discussed earlier, this behavior in the cubic phase is consistent with the lowering of the phonon symmetry from F_{2u} to F_2 by the relaxation of inversion symmetry.

For this geometry, the relaxation of translational symmetry may account for all the three forbidden lines in the ferroelectric phase. There are a multiplicity of symmetry points in the Brillouin zone that could contribute to the $X(yx)Y$ spectrum, depending upon the single-phonon density of states. Since density-of-states information is not available, an attempt to associate the observed structure with phonons at a particular symmetry point is not meaningful.
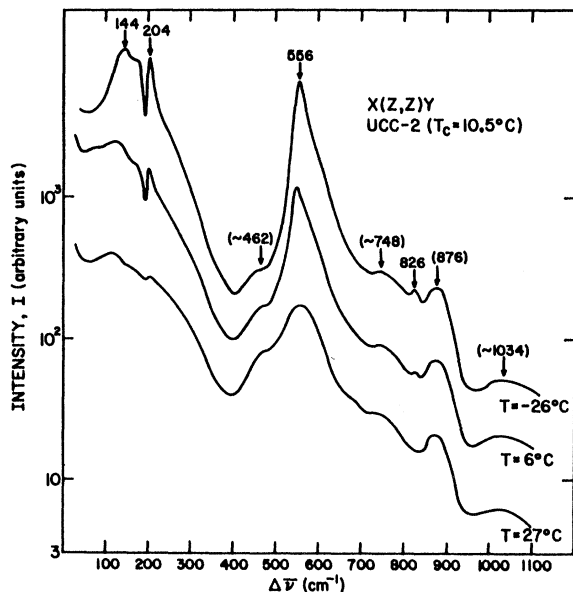
FIG. 9. $X(zz)Y$ spectrum measured at three different temperatures. The curves are not referred to the same baseline. Higher-order bands are identified with parentheses.
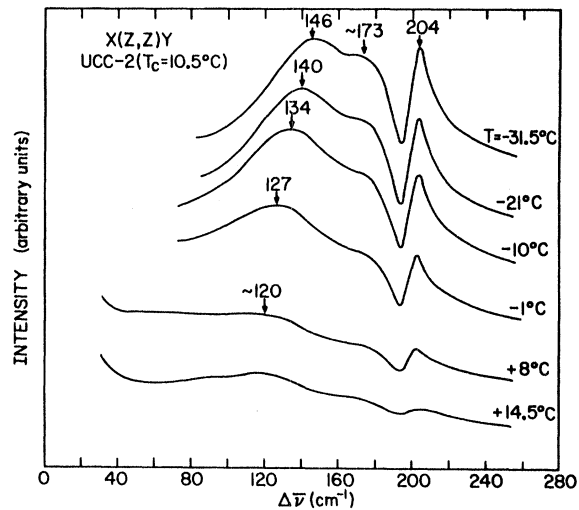
FIG. 10. Temperature dependence of the $X(zz)Y$ spectrum for $80 < \Delta\bar{\nu} < 260$ cm^{-1}. The curves are not referred to the same baseline.

B. $A_{1 TO}$-Symmetry Modes

The $X(zz)Y$ spectrum is shown in Fig. 9. According to the selection rules, only phonons with $A_{1 TO}$ symmetry are first-order active for this spectrum. The intensity of the second-order background is found to be 20–30 times more intense than that of the $X(zx)Y$ spectrum. The second-order intensity of $KTaO_3$ shows a similar behavior. The first-order lines at 825, 556, and 204 cm^{-1} are degenerate with E-symmetry phonons which were observed in the $X(zx)Y$ spectrum. The temperature dependence of the 204-cm^{-1} peak, shown more clearly in Fig. 10, is similar to that observed in the $X(zx)Y$ spectrum, showing a residual structure in the paraelectric phase and the interference effect with the two-acoustical-phonon continuum. The line at 556 cm^{-1} exhibits a behavior similar to that observed in the $X(zx)Y$ spectrum and the same interpretation applies. These results are discussed in more detail later. In the spectra shown in Fig. 9, there is no evidence of structure at 419 and 279 cm^{-1}, where lines are seen in the E-symmetry spectra shown in Fig. 2. The signal-to-noise ratio in these spectral regions is sufficient to have observed first-order $A_{1 TO}$ structure, particularly for the case of the 279 cm^{-1}, if it were present. The band at 144 cm^{-1} seen in Fig. 9 is not degenerate with the E mode in the corresponding spectral regions but appears with a frequency approximately 10 cm^{-1} greater. This line also shows a temperature-dependent frequency as shown in Fig. 10. The frequency decreases with increasing temperature at the rate of approximately 0.5 cm^{-1}/°C, with the peak merging finally into
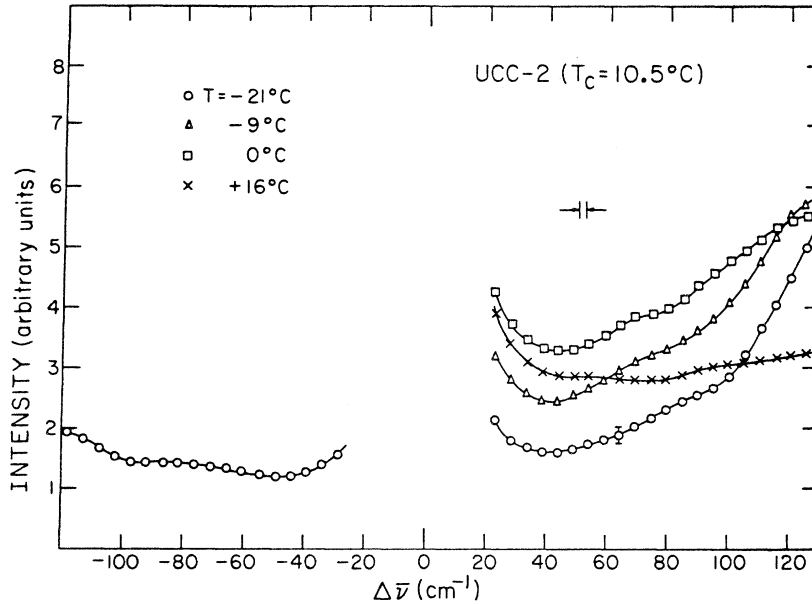
FIG. 11. $X(zz)Y$ spectrum for $|\Delta\bar{\nu}| < 120$ cm^{-1}. The spectral slit used was ≈ 2 cm^{-1}.

the two-phonon band at 120 cm^{-1}.

Soft $A_{1\,TO}$ mode. The low-frequency portion of the $X(zz)Y$ spectrum measured with a small spectral slit is shown in Fig. 11. The general increase of the intensity with increasing temperature in this spectral region in the ferroelectric phase is largely due to the shift of the 144-cm^{-1} band to lower frequencies at higher temperatures. At $T = -21$ °C, there is a broad, weak structure at approximately 85 cm^{-1} in both the Stokes and anti-Stokes spectra. This band shows a temperature-dependent frequency and shifts to ≈ 70 cm^{-1} at $T = 0$ °C. The soft ferroelectric mode should have an $A_{1\,TO}$ component, which, according to the modified Lyddane-Sachs-Teller relations for a uniaxial crystal[31]

$$\frac{\epsilon_0^a}{\epsilon_\infty^a} = \prod_{j=1}^{4} \left(\frac{\omega_{E\,LO}(j)}{\omega_{E\,TO}(j)}\right)^2 \quad , \quad \frac{\epsilon_0^c}{\epsilon_\infty^c} = \prod_{j=1}^{3} \left(\frac{\omega_{A1\,LO}(j)}{\omega_{A1\,TO}(j)}\right)^2 \quad ,$$

$$\tag{2}$$

should have a higher frequency than the E_{TO} component, since ϵ_0^c is much smaller than ϵ_0^a and $\epsilon_\infty^c \approx \epsilon_\infty^a$. Further, since the E_{TO} mode is heavily damped, the A_{1TO} mode might be expected to show considerable damping and appear in the Raman spectrum as a rather broad structure. Therefore the structure at 85 cm^{-1} at $T = -21$ °C will be tentatively assigned to the soft A_{1TO} mode and the quasimode spectrum will be examined for confirming evidence.

As discussed previously, the quasimodes are phonons of mixed A_1 and E symmetry propagating along a direction inclined at an angle from the z axis. The frequency of the quasimodes shows a

directional dispersion which has been treated theoretically by Merten[32] and by Loudon.[15] The treatment of Merten is the more accurate but is rather complex. The simpler result of Loudon is sufficient for the accuracy that is obtainable here. According to Loudon, the frequency of the transverse quasimode is given by

$$\omega_{QTO}^2 = \omega_{ETO}^2 \cos^2\theta + \omega_{A1\,TO}^2 \sin^2\theta \tag{3}$$

and the frequency of the longitudinal quasimode by

$$\omega_{QLO}^2 = \omega_{ELO}^2 \sin^2\theta + \omega_{A1\,LO}^2 \cos^2\theta \tag{4}$$

for the approximation that the electrostatic forces dominate the lattice forces. The angle θ is the angle between the phonon wave vector and the z axis. The value of ≈ 35 cm^{-1} for the frequency assigned to the soft E_{TO} mode and the value of 85 cm^{-1} assigned to the soft $A_{1\,TO}$ mode give, according to Eq. (3), an expected value of ≈ 65 cm^{-1} for the frequency of the transverse quasimode in the $Z(yy)X$ spectrum. In the measured $Z(yy)X$ spectrum shown in Fig. 12, a weak, but well-defined, peak is observed at 65 cm^{-1} as expected. Thus, the soft-mode assignments appear to be justified.

One other feature of interest in the $Z(yy)X$ spectrum shown in Fig. 12 is the peak at 275 cm^{-1}, which is assigned to the B_1 component of the silent mode.

C. Summarizing Comments

The results of the scattering measurements are summarized in Table II. In this table are listed the energy shift of the various Raman lines assigned to either first- or second-order scattering.
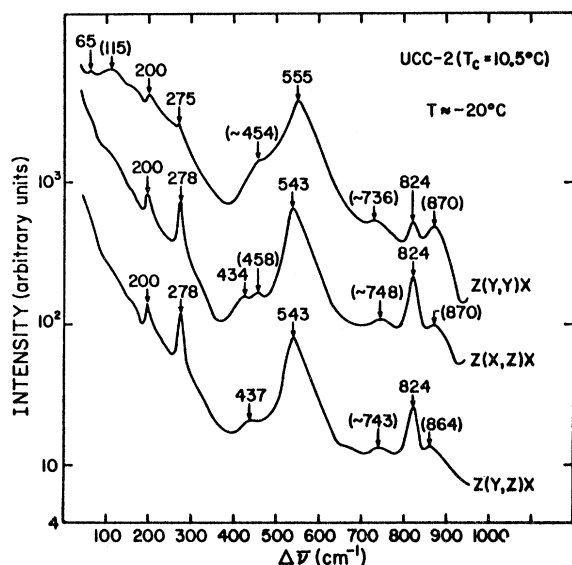
FIG. 12. $Z(yy)X$, $Z(xz)X$, and $Z(yz)X$ spectra at T = −20 °C. The curves are not referred to the same baseline. Higher-order bands are identified with parentheses.

The phonon symmetry, transverse or longitudinal character, and the phonon-branch index assignment in order of frequency are listed for each Raman line. For example, a transverse phonon with A_1 symmetry assigned to branch 2 is listed as $A_{1\,TO\,2}$. The indices 1, 2, and 4 correspond to the cubic F_{1u} modes, and the index 3 is associated with the cubic F_{2u} mode. In the first-order column, a sum, for example, $A_{1\,TO\,4} + E_{TO\,4}$, indicates degenerate phonons. In the second-order column, the notation $2TO_4$ or $TO_4 + TO_2$, for example, is used to indicate overtone or combination two-phonon bands, respectively. The assignments enclosed by brackets are not based on direct observation but are expected from a comparison with results of measurements on other perovskites. The assignments enclosed by curly braces are speculative. The data for KTaO$_3$ are listed for comparison. For KNbO$_3$, the available data are very limited. In the Raman measurements on multidomain KNbO$_3$ in the tetragonal phase,[9] only two peaks—at 292 and 838 cm^{-1}—can be definitely assigned as first-order Raman lines.

Inspection of Table II shows that there is a close correspondence between both the frequency and symmetry of the phonons in KTN and those of KTaO$_3$, indicating that the Raman spectrum of this mixture of KTN is predominantly that of the host lattice of KTaO$_3$. The frequencies of the second-order bands in the two materials are very close. The phonon assignments of the second-order spectra in KTN were made by a comparison with the KTaO$_3$ results.

The first-order phonon spectrum of KTN shows

some important differences with the KTaO$_3$ spectrum. The line at 826 cm^{-1} shows well-defined, degenerate $A_{1\,TO} + E_{TO} + F$ character, where F represents the forbidden symmetry structure observed in the $X(yx)Y$ spectrum. The infrared results in KTaO$_3$ show an LO phonon near this frequency shift. The results of measurements (both infrared and Raman) in other of the pure perovskites indicate that the highest-frequency first-order line should be an LO mode. Accordingly, it is indicated in Table II that this line should probably contain contributions from LO$_4$ phonons. The TO + F character observed is apparently an anomalous behavior due to the mixed nature of the crystal. It should be pointed out, however, that the LO$_4$ mode appearing at ≈ 720 cm^{-1} in the BaTiO$_3$ spectrum[17] also shows anomalies, appearing in some spectra in which it should be forbidden by the selection rules.

The silent mode at 279 cm^{-1} shows $E_{TO} + F$ symmetry, with the B_1-symmetry component shifted slightly to 275 cm^{-1}. From a comparison with results on other perovskites, the 279-cm^{-1} line probably contains a degenerate E_{LO} contribution as indicated. Since this mode is not infrared active in the cubic phase, the LO, TO splitting is expected to be quite small. The silent modes which appear at 305 cm^{-1} in BaTiO$_3$[17] and at 290 cm^{-1} in PbTiO$_3$[18] show no LO, TO splitting also. Note that the silent mode has not been observed by any technique in KTaO$_3$. Considering the close correspondence of phonons, it can be expected from the results on KTN that the frequency of the silent mode in pure KTaO$_3$ is ≈ 279 cm^{-1}. This demonstrates a potential usefulness of Raman studies in mixed-crystal systems as a means of obtaining information that might be otherwise inaccessible.

The 202-cm^{-1} line shows degenerate $A_{1\,TO\,2} + E_{TO\,2} + F$ character. Neglecting the F contribution, this agrees well with the induced Raman and infrared results for KTaO$_3$. The infrared data for KTaO$_3$ show that the LO$_1$ mode at approximately 188–196 cm^{-1} is nearly degenerate with the TO$_2$ phonon. Thus, it is indicated in Table II that there may be some LO$_1$ contribution to the 202-cm^{-1} line of KTN.

Besides the three lines having forbidden symmetry, the following results arise from the departure of KTN from a pure perovskite. The neutron scattering data show that the energy of the TO$_1$ phonon in KTaO$_3$ at the zone boundary is 175 cm^{-1}. It is possible, therefore, that the structure at 175 cm^{-1} seen in Figs. 3 and 10 is due to the zone-boundary TO$_1$ mode which is made first-order Raman active by the relaxation of translational symmetry. The 436-cm^{-1} line seen in Fig. 2 may also be due to a zone-boundary phonon. The second-order 2LO$_2$ band at 870 cm^{-1} in KTN appears at approximately twice the frequency

TABLE II. Symmetry and branch assignments of the optical phonons in KTN.

| KTN, $T = -20°C$ | | | | KTaO$_3$, $T = 30°C$ | |
First order	Second order	First-order induced Raman[a]	Infrared[b]	Second-order Raman[c]	Zone-boundary phonon energy[d]
	1720, 2LO$_4$			1748, 2LO$_4$	
	1040, 2TO$_4$			1095, 2TO$_4$	
	870, 2LO$_2$			886, 2LO$_2$	
826, $A_{1TO}+E_{TO}+F$ +[LO$_4$]			833, LO$_4$		
	748, TO$_4$+TO$_2$			738, TO$_4$+TO$_2$	
	690, TO$_4$+TO$_1$			692, TO$_4$+TO$_1$	
	560, TO$_4$+TA			589, TO$_4$+TA	
555, $A_{1\,TO4}+E_{TO4}$		556, $A_{1\,TO4}$	549, TO$_4$		
	464, TO$_4$ – TA			465, TO$_4$ – TA	
436, {ZB LO$_2$}					
419, E_{LO2}			423, LO$_2$		
279, $E_{TO3}+F$ +[E_{LO3}]					
275, B_1				271, TO$_1$+TA	
202, $A_{1\,TO2}+E_{TO2}+F$ +[LO$_1$]		198, $A_{1\,TO2}$	199, TO$_2$		195, TO$_2$
			188–196, LO$_1$		
175, {ZB TO$_1$}					175, TO$_1$
				160, TO$_1$ – TA	
140, $A_{1\,TO}$					
130, E_{LO}					
	120, 2TA			123, 2TA	
85, $A_{1\,TO1}$		85, $A_{1\,TO1}$	85, TO$_1$		
					65, TA
35, E_{TO1} wing					

[a]From Ref. 12. At room temperature, only the $A_{1\,TO}$ modes were observed.
[b]From Ref. 29 and R. C. Miller and W. G. Spitzer, Phys. Rev. 129, 94 (1963).
[c]From Ref. 22.
[d]From neutron-diffraction data (see Ref. 30).

of the 436-cm^{-1} line. There is no corresponding structure in the KTaO$_3$ data. Thus, as indicated in the table, it appears reasonable to attribute the 436-cm^{-1} line to the zone-boundary LO$_2$ phonon. The persistence of both of these lines in the paraelectric phase is consistent with this assignment.

For the ideal perovskite structure, there should be a maximum of three $A_{1\,TO}$ modes. Excluding the 826-cm^{-1} line, which is showing anomalous behavior, these are accounted for by the lines at 85, 202, and 55 cm^{-1} in KTN, in good agreement with the KTaO$_3$ spectrum. The $A_{1\,TO}$ mode appearing at 140 cm^{-1} is apparently an extra line. There is no structure in the KTaO$_3$ results corresponding to either the $A_{1\,TO}$ mode at 140 cm^{-1} or the E_{LO} mode at 130 cm^{-1} in the KTN spectrum. These two lines apparently arise from local modes associated with the Nb ions.

It is considered to be a general trend in mixed-crystal systems[20,33] that, if the energies of corresponding phonon branches in the constitutent materials are not too different, a single line will appear in the Raman spectrum at a frequency intermediate to those of the constituents, and local modes are not expected. This is called "one-mode"

behavior. If the energies of corresponding phonon branches are well separated, then the tendency is for local modes to occur and one observes "two-mode" behavior. In general, the phonon energies of the perovskites are similar. Although, as pointed out earlier, there is only a limited amount of information available for KNbO$_3$, it does not appear that KTaO$_3$ and KNbO$_3$ are an exception in this respect. Therefore, one would expect one-mode behavior in the mixed perovskites rather than the apparent two-mode behavior observed here.

V. ELECTRIC-FIELD-INDUCED RAMAN SCATTERING

A. General Discussion

An electric field applied along a crystal axis of a perovskite material in the cubic phase lowers the crystal symmetry from O_h to C_{4v}. The lowered symmetry is the same as that of the tetragonal ferroelectric phase, so that the effect of the electric field is to induce first-order Raman activity above the transition temperature in the paraelectric phase. Induced first-order Raman scattering in cubic KTaO$_3$ and SrTiO$_3$ has been observed by using both pulsed and ac field modulation.[11,12] There

have been no induced-scattering measurements in the cubic phase of a material which shows a phase transition to compare the induced first-order intensity with the spontaneous first-order intensity in the ferroelectric phase.

It has been found in studies of the spontaneous and induced splitting of the absorption edge in KTN[34] that, for the edge splitting, the important ionic displacements associated with an induced polarization in the paraelectric phase were similar in both magnitude and character to those occurring spontaneously in the ferroelectric phase for the same value of spontaneous polarization. It is reasonable to expect, therefore, that the induced Raman intensity in the paraelectric phase should be comparable to the spontaneous intensity in the ferroelectric phase for comparable polarization.

Theoretical calculations of the scattering efficiency of the soft ferroelectric mode have been made by Dvořák[13] and, more recently, by Wemple and DiDomenico.[14] The calculation of Wemple and Di-Domenico relates the scattering efficiency of the soft mode to fluctuations in the optical dielectric-constant tensor which are induced by fluctuations of the lattice polarization existing in the crystal. The calculation applies to both spontaneous scattering in the ferroelectric phase and induced first-order scattering in the paraelectric phase. Their final results for the scattering efficiencies are

$$S_{33} \propto T \epsilon_c P^2, \quad S_{42} \propto T \epsilon_a P^2, \tag{5}$$

where S_{33} is the scattering efficiency for the zz components of the soft $A_{1\,TO}$ mode, S_{42} is the scattering efficiency for the soft E_{TO} mode, T is the absolute temperature, P is the lattice polarization along the z axis, and ϵ_c and ϵ_a are the c- and a-axis static dielectric constants, respectively. Temperature- and field-independent proportionality constants are omitted in Eqs. (5). According to Eqs. (5), the scattering efficiencies just above and below the transition temperature should be approximately equal for comparable polarization, since, according to the Devonshire theory,[35] the dielectric constants in the two phases should be comparable for these conditions. The treatment of Dvořák gives a result which is the same in the limit of small fields where $\epsilon_a \approx \epsilon_c$. It should be emphasized that these calculations apply only to the soft modes. Dvořák, however, estimates that the scattering efficiency of the other phonons of frequency ω_i is reduced by approximately the ratio $(\omega_{soft}/\omega_i)^2$ and has approximately the same polarization dependence.

The first-order Raman scattering in the paraelectric phase of KTN was induced by applying a dc electric field to the crystal and also by using the ac-field-modulation technique. The ac field modulation has the advantage that the intense second-order background can be eliminated. According to Eqs. (5), the scattered intensity of the field-induced first-order scattering is proportional to P^2, where P is induced by an electric field. With $E_{appl} = E_0 \sin \omega t$, the scattered intensity I_s is (neglecting saturation effects)

$$I_s \propto E_0^2 \sin^2 \omega t = E_0^2 (1 - \cos 2\omega t) . \tag{6}$$

The induced first-order intensity is thus modulated at $2\omega t$. The second-order scattering intensity remains nearly constant at the phase transition; therefore it is not sensitive to the electric field. By using synchronous detection and tuning the lock-in amplifier to $2\omega t$, the dc second-order scattering is rejected (the laser light is not chopped), and only the induced signal is detected.

Two complications involved in the measurements with an applied ac field should be considered. It was found that the applied ac field caused a small mechanical vibration of the sample on the tailpiece of the Dewar which, in turn, produced a modulation of the scattered light intensity as it passed through the monochromator system. The modulation occurred at both the first- and second-harmonic frequencies of the applied field. It was determined that this spurious contribution was caused primarily by the shifting of the image of the exit slit of the first monochromator on the entrance slit of the second monochromator and could be made negligible by operating with wide slits on the second monochromator. The results presented later were obtained in this manner, so that the contribution of this spurious signal to the measured results was negligible. The necessity of using wide slits precluded any investigation of induced scattering from the soft ferroelectric modes.

A second complication was associated with the second-order scattering which was modulated at $2\omega t$ but shifted 180° out of phase with the induced first-order scattering. As pointed out above, an electric field should not affect the second-order scattering process. The field, however, may modulate the optical constants of the medium through which the scattered light is passing, so that the measured intensity outside of the sample is modulated. It will be shown that a modulation of the absorption coefficient in the spectral region of interest is to be expected, and that this effect contributed to the observed results. A small change of the index of refraction may also be expected; it was determined, however, that this effect alone is small and would predict a steadily increasing second-harmonic intensity for decreasing $\Delta \bar{\nu}$ in contrast to the observed results.

It has been observed that, for $h\nu < 3$ eV, an applied electric field in the paraelectric phase of KTN produced a small increase in the absorption coefficient with $\Delta \alpha_\parallel \gtrsim \Delta \alpha_\perp$.[34] A similar effect pro-

duced by the spontaneous polarization was observed in ferroelectric, semiconducting KTN[36] in the spectral region between an interband absorption edge and the impurity absorption band present in those samples. Theoretically, Tharmalingam[37] has shown that a uniform electric field will produce an increase in the absorption coefficient below the interband edge by a tunneling effect of the Franz-Keldysh type. The effect of an increase in the absorption coefficient on the observed scattered light for 90° scattering can be estimated as follows. Let I_l be the intensity of the incident laser light. The intensity of the exciting light at the center of a sample of length $2d$ is

$$I'_l = I_l \frac{(1-R)e^{-\alpha d}}{1 - Re^{-2\alpha d}} , \tag{7}$$

where α is the absorption coefficient and R is the reflectivity. The intensity of the observed scat-

FIG. 13. Upper half: Curve 1 represents the spontaneous first-order Raman scattering at $T - T_c = -2.5\,°C$ in the single-domain-ferroelectric phase; curve 2 represents the second-order scattering at $T - T_c = +24.5\,°C$ with no applied field in the paraelectric phase. Lower half: Second-harmonic intensity of ac-modulated, induced first-order scattering in the paraelectric phase. The dashed curve is the calculated intensity of the modulated background scattering. Curve 3 is the measured second-harmonic intensity for $P = 3.2\ \mu C/cm^2$. Curve 4 is the measured second-harmonic intensity for $P = 5.8\ \mu C/cm^2$.

tered light is given by

$$I = bI'_l \frac{(1-R)e^{-\alpha x}}{1 - Re^{-2\alpha x}} , \tag{8}$$

where b is proportional to the scattering efficiency and $2x$ is the width of the sample. Let α_0 be the zero-field absorption coefficient and $\alpha_0 + \Delta\alpha$ be the absorption coefficient with an electric field applied to the sample. Neglecting the change of R, the observed scattering intensity with a field E applied to the sample can be written, for $\Delta\alpha \ll 1$, as

$$I(E) \approx I_0 [1 - (x+d)\Delta\alpha] , \tag{9}$$

where I_0 is the observed scattering intensity for $E = 0$. Since $\Delta\alpha$ increases with $|\vec{E}|$, it can be written as

$$\Delta\alpha = aE_0 |\sin\omega t| \tag{10}$$

for an ac electric field, giving

$$I = I_0 \left(1 - \frac{2a(x+d)E_0}{\pi} + \frac{4a(x+d)E_0}{3\pi} \cos2\omega t + \cdots \right). \tag{11}$$

This equation shows that, owing to $\Delta\alpha$, a second-harmonic intensity is contributed by the second-order scattering, and that the contribution is 180° out of phase with the induced first-order signal [see Eq. (6)]. This effect is serious when the second-order scattering is comparatively strong. The field produced $\Delta\alpha$ also reduces directly the intensity of the first-order induced scattering; however, this reduction is estimated to be less than $\approx 6\%$ and will be neglected.

B. Results

Induced first-order scattering was investigated in the spectral region $\Delta\bar{\nu} < 300\ cm^{-1}$ in which strong, isolated, first-order peaks occur in the ferroelectric phase. The results of the induced-scattering measurements at $T - T_c = 24.5\ °C$ are shown in Fig. 13. The upper part of the figure shows curves measured without an applied field. Curve 1 was measured in the ferroelectric phase, at 2.5 °C below the transition temperature. Curve 2 refers to the paraelectric phase with no applied field. These spectra were measured with spectral slits of ≈ 12 and $\approx 120\ cm^{-1}$ for the first and second monochromators, respectively. The rapidly increasing intensity for $\Delta\bar{\nu} < 100\ cm^{-1}$ is due to spuriously scattered Rayleigh light. No measurable change from curve 2 could be observed when a dc electric field of magnitude sufficient to induce a polarization of $\approx 6\ \mu C/cm^2$ was applied to the sample.

The results of the scattering measurements made under an applied ac field at $T - T_c = 24.5\ °C$ are shown by the solid curves 3 and 4 in the lower portion of Fig. 13. The dashed curve is the calculated intensity of the second-order scattering modulated
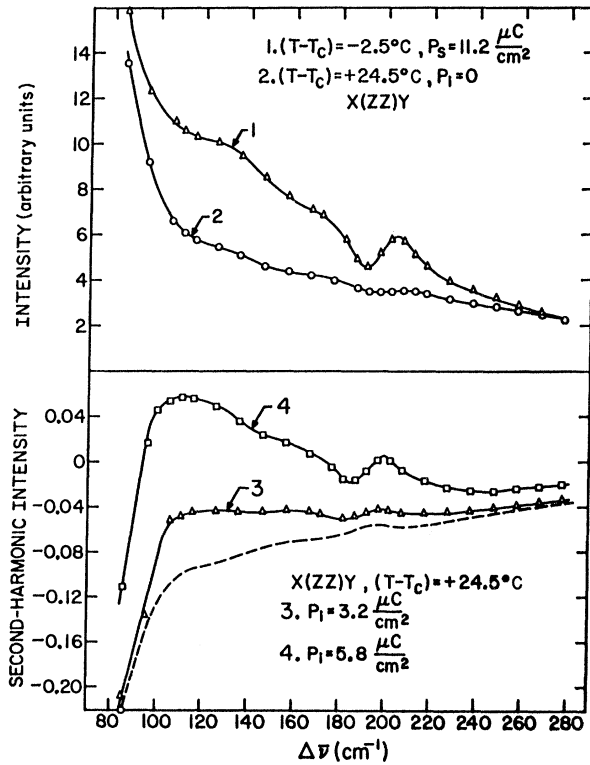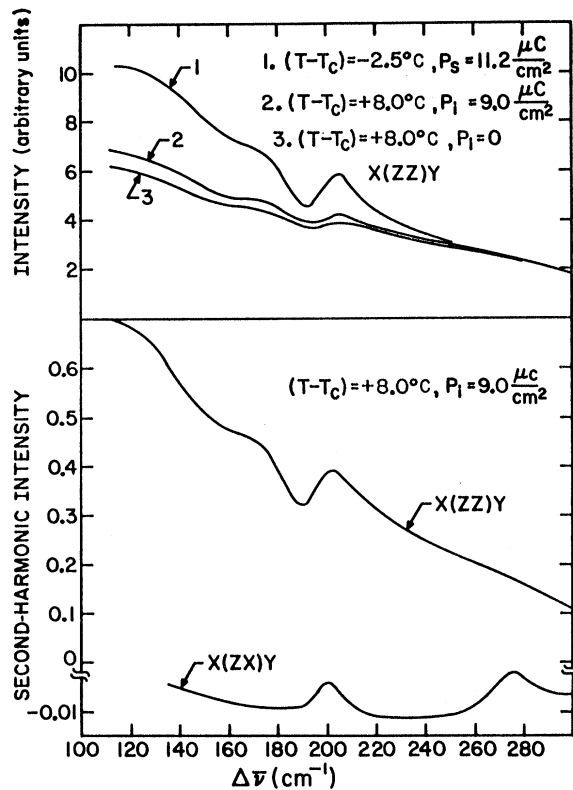
FIG. 14. Upper half: Curve 1 represents the spontaneous first-order Raman scattering at $T - T_c = -2.5\,°C$ in the single-domain-ferroelectric phase; curve 2 is the scattering in the paraelectric phase at $T - T_c = +8.0\,°C$ with an induced dc polarization of 9.0 $\mu C/cm^2$; curve 3 is the second-order scattering with no applied field at $T - T_c = +8.0\,°C$. Lower half: Second-harmonic intensity of ac-modulated, first-order scattering for the $X(zz)Y$ and $X(zx)Y$ spectra at $T - T_c = +8.0\,°C$ and $P = 9.0\ \mu C/cm^2$.

at $2\omega t$ by $\Delta\alpha$, for an induced polarization of 3.2 $\sin\omega t\ \mu C/cm^2$. The curve was calculated using Eq. (11) and the measured second-order scattering shown by curve 2 in the upper part of the figure. At $\Delta\bar\nu \approx 280\ cm^{-1}$, the calculated curve and the measured curve 3 nearly coincide, showing that there is no induced first-order contribution in this region. This agreement also justifies the neglect of ΔR in obtaining Eq. (9). The difference between the two curves gives the induced first-order scattering. At $\Delta\bar\nu \approx 100\ cm^{-1}$, the modulated Rayleigh signal becomes dominant, and the signal rapidly becomes negative. The measured results for an

induced polarization of 5.8 $\mu C/cm^2$ are shown by curve 4. The induced first-order peak at $\approx 200\ cm^{-1}$ and the first-order structure between 100 and 180 cm^{-1} are clearly evident in this curve. The difference between curve 4 and the second-harmonic signal of the second-order scattering calculated for $P = 5.8\ \mu C/cm^2$ shows that the total induced first-order scattering intensity is a few percent of the zero-field scattering shown by curve 2. Thus, the ac field measurements are consistent with the result that no measurable change could be detected with a dc applied field.

Measurements of the induced scattering were also made at a lower temperature. Figure 14 shows the results of measurements at $T - T_c = 8.0\,°C$. Curves 1 and 3 were measured in the ferroelectric and paraelectric phases, respectively, with no applied electric field. Curve 2 gives the $X(zz)Y$ spectrum with an applied dc field, after a correction for $\Delta\alpha$. At this temperature, a higher dc polarization could be induced, and some indication of first-order scattering could be observed. The curves in the lower half of Fig. 14 give the induced scattering calculated from the second-harmonic intensity measured with an applied ac field. The curve for $X(zz)Y$ is consistent with the indication of dc measurements. The curve for $X(zx)Y$ shows induced E_{TO} modes at 200 and 279 cm^{-1}. The structure at 279 cm^{-1} is absent in the $X(zz)Y$ spectrum as required by the selection rules. The field corresponding to a polarization of 9.0 $\mu C/cm^2$ induced a change in the intensity of the 200-cm^{-1} peak which was approximately 17% of the peak intensity of the line measured in the ferroelectric phase at a spontaneous polarization of 11.2 $\mu C/cm^2$. Corrected by the factor $(P_s/P_{ind})^2$, the induced intensity is ≈ 0.25 that of the spontaneous intensity for the same polarization.

The existing theories would predict that the induced scattering, particularly from the $A_{1\,TO}$ modes, should be somewhat greater than the spontaneous scattering for the same polarization, since $(T\epsilon_c)_{para} > (T\epsilon_c)_{ferro}$ for the temperatures used. The proportionality constants omitted in Eqs. (5) involve zero-field indices of refraction. The change in the indices of refraction produced by the spontaneous polarization at the phase transition is only of the order of 2–3%,[38] which is not sufficient to account for the observed difference in the scattered intensities. The comparatively low intensity of induced scattering presents an interesting problem for further investigation.

---

[1]W. Cochran, Advan. Phys. 9, 387 (1960).

[2]P. W. Anderson, in *Proceedings of the All-Union Conference on the Physics of Dielectrics* (Academy of Sciences, USSR, Moscow, 1958), p. 290.

[3]G. Burns and B. A. Scott, Phys. Rev. Letters 25, 1191 (1970); Bull. Am. Phys. Soc. 16, 29 (1971); 16, 415 (1971).

[4]W. J. Brya, Phys. Rev. Letters 26, 1114 (1971).

[5]R. T. Harley, J. B. Page, Jr., and C. T. Walker, Phys. Rev. Letters 23, 922 (1969).

[6]A. R. Evans and D. B. Fitchen, Phys. Rev. B 2, 1074 (1970).

[7]I. Nair and C. T. Walker, Bull. Am. Phys. Soc. 16, 28 (1971).

[8]L. T. Todd, Jr., M. S. thesis (MIT, Cambridge, Mass., 1970) (unpublished).

[9]C. H. Perry and N. E. Tornberg, in Light Scattering Spectra of Solids, edited by G. B. Wright (Springer, Berlin, 1969), p. 467.

[10]T. G. Davis, J. Phys. Soc. Japan Suppl. 28, 245 (1970).

[11]P. A. Fleury and J. M. Worlock, Phys. Rev. Letters 18, 665 (1967).

[12]P. A. Fleury and J. M. Worlock, Phys. Rev. 174, 613 (1968).

[13]V. Dvořák, Phys. Rev. 159, 652 (1967).

[14]S. H. Wemple and M. DiDomenico, Jr., in Light Scattering Spectra of Solids, edited by G. B. Wright (Springer, Berlin, 1969), p. 65.

[15]R. Loudon, Advan. Phys. 13, 423 (1964).

[16]H. Poulet, Ann. Phys. (Paris) 10, 908 (1955).

[17]M. DiDomenico, Jr., S. H. Wemple, S. P. S. Porto, and R. P. Bauman, Phys. Rev. 174, 522 (1968).

[18]G. Burns and B. A. Scott, Phys. Rev. Letters 25, 167 (1970).

[19]A. A. Maradudin, in Localized Excitations in Solids, edited by R. F. Wallis (Plenum, New York, 1968), p. 1.

[20]A. S. Barker, Jr., in Localized Excitations in Solids, edited by R. F. Wallis (Plenum, New York, 1968), p. 581.

[21]J. M. Worlock and S. P. S. Porto, Phys. Rev. Letters 15, 697 (1965).

[22]W. G. Nilsen and J. G. Skinner, J. Chem. Phys. 47, 1413 (1967).

[23]W. G. Nilsen and J. G. Skinner, J. Chem. Phys. 48, 2240 (1968).

[24]D. L. Rousseau and S. P. S. Porto, Phys. Rev. Letters 20, 1354 (1968).

[25]U. Fano, Phys. Rev. 124, 1866 (1961).

[26]U. Fano and J. W. Cooper, Phys. Rev. 137, A1364 (1965).

[27]A. Pinczuk, E. Burstein, and S. Ushioda, Solid State Commun. 7, 139 (1969).

[28]A. S. Barker, Jr. and J. J. Hopfield, Phys. Rev. 135, A1732 (1964).

[29]A. S. Barker, Jr., Phys. Rev. 145, 391 (1966).

[30]G. Shirane, R. Nathans, and V. J. Minkiewicz, Phys. Rev. 157, 396 (1967).

[31]W. Cochran and R. A. Cowley, J. Phys. Chem. Solids 23, 447 (1962).

[32]L. Merten, Phys. Status Solidi 25, 125 (1968); also Z. Naturforsch. 22a, 359 (1967).

[33]G. Lucovsky, M. Brodsky, and E. Burstein, in Localized Excitations in Solids, edited by R. F. Wallis (Plenum, New York, 1968), p. 592.

[34]S. K. Manlief and H. Y. Fan (unpublished).

[35]A. F. Devonshire, Phil. Mag. 40, 1040 (1949); also Advan. Phys. 3, 85 (1954).

[36]M. DiDomenico, Jr. and S. H. Wemple, Phys. Rev. 166, 565 (1968).

[37]K. Tharmalingam, Phys. Rev. 130, 2204 (1963).

[38]J. A. van Raalte, J. Opt. Soc. Am. 57, 671 (1967).

Optical Absorption and Thermoluminescence of X-Ray-Irradiated KBr Crystals at Room Temperature

G. T. Hageseth

The University of North Carolina, Greensboro, North Carolina 27412

Two thermoluminescence peaks are observed in KBr crystals that are x irradiated at room temperature. The 185 °C peak can be removed by annealing the crystal for several hours at 400 °C and is attributed to highly localized defects. The 152 °C peak is proposed to be due to the liberation and recombination of the electrons from the F centers. The single glow peak obtained at 152 °C is analyzed by the area method and initial-rise method to give thermal trap depths of 0.55 ± 0.04 and 0.61 ± 0.02 eV, respectively. The optical absorption measurements indicate that F and V_2 centers are formed in the crystal during the x-irradiation process. The thermoluminescence spectra has been analyzed to consist of one narrow emission band centered at 3.08 eV. This thermoluminescence process is found to be nearly first order and an energy-level diagram is proposed to correlate the optical absorption and emission spectra.

I. INTRODUCTION

Mehendru and Radhakrisha[1] have previously reported thermoluminescence (TL) of pure and impurity-doped KBr crystals. Two types of F centers[2–10] have been postulated to explain a variety of experimental data. The fast stage of F centers are the ones formed by electrons trapped at anion vacancies initially present in the crystals, whereas the slow stage are electrons trapped at anion vacancies created during the x-irradiation process. Jain and Mehendru[10] have postulated an intimate correlation between the growth of the F centers and the growth of the areas under the thermoluminescence peaks in KCl. In KCl crystals a heating rate of 40 °C min⁻¹ gave two peaks at 135 and 190 °C and have been inter-